

Coordination studies of 5,6-diphenyl-3-(2-pyridyl)-1,2,4-triazine towards Cu^{2+} cation. X-ray studies, spectroscopic characterization and DFT calculations

B. Machura^{a,*}, A. Świtlicka^a, R. Kruszynski^b, J. Mroziński^c, J. Kłak^c, J. Kusz^d

^a Department of Crystallography, Institute of Chemistry, University of Silesia, 9th Szkolna Street, 40-006 Katowice, Poland

^b Department of X-ray Crystallography and Crystal Chemistry, Institute of General and Ecological Chemistry, Lodz University of Technology, 116 Żeromski Street, 90-924 Łódź, Poland

^c Faculty of Chemistry, Wrocław University, F. Joliot-Curie 14 Street, 50-383 Wrocław, Poland

^d Institute of Physics, University of Silesia, 4th Uniwersytecka Street, 40-006 Katowice, Poland

ARTICLE INFO

Article history:

Received 21 April 2008

Accepted 25 May 2008

Available online 7 July 2008

Keywords:

Copper complexes

5,6-Diphenyl-3-(2-pyridyl)-1,2,4-triazine

X-ray and electronic structure

DFT calculations

ABSTRACT

The reactions of 5,6-diphenyl-3-(2-pyridyl)-1,2,4-triazine with $\text{CuCl}_2 \cdot 2\text{H}_2\text{O}$, $\text{Cu}(\text{NO}_3)_2 \cdot 3\text{H}_2\text{O}$ and $\text{CuSO}_4 \cdot 5\text{H}_2\text{O}$ have been examined, and four $[\text{CuCl}_2(\text{dppt})]$ (**1**), $[\text{CuCl}_2(\text{dppt})_2] \cdot 2\text{MeOH}$ (**2**), $[\text{Cu}(\text{dppt})_2(\text{H}_2\text{O})_2](\text{NO}_3)_2$ (**3**) and $[\text{Cu}(\text{SO}_4)(\text{dppt})(\text{H}_2\text{O})]_n \cdot n\text{H}_2\text{O}$ (**4**) complexes have been obtained. All the complexes have been structurally and spectroscopically characterized, and compound **4** has been additionally studied by magnetic measurements. The electronic structure of **1** has been calculated with the density functional theory (DFT) method, and the time-dependent DFT calculations have been employed to calculate the electronic spectrum of **1**.

© 2008 Elsevier Ltd. All rights reserved.

1. Introduction

Numerous compounds containing the 1,2,4-triazine moieties are well known in natural materials and show interesting biological, pharmacological and medicinal properties. 4-amino-5-oxo-3-phenylamino-1,2,4-triazine has a powerful inhibiting effect on the cell wall lignification catalysed by peroxidases, and alters the integrity of chloroplast [1]. Some of the 3,5,6-trisubstituted-1,2,4-triazines can be active as blood platelet aggregation inhibitors and others exhibit antiviral inhibitory activity (against influenza viruses for example), significant activity towards leukaemia and ovarian cancer, and anti-HIV activity [2]. More recently, it has been revealed that a zinc-dppt complex (dppt = 5,6-diphenyl-3-(2-pyridyl)-1,2,4-triazine) associated to a biocide could have significant biocidal effects on living cells including those of microorganisms (bacteria and fungi), cell culture system, plants and animals [3].

Another interesting property of the derivatives of 1,2,4-triazine compounds is formation of coloured complexes when they are coordinated to a metal ion. In particular, the ligand 5,6-diphenyl-3-(2-pyridyl)-1,2,4-triazine has been widely used as a sensitive reagent for the determination of Fe(II) by spectrophotometric methods, in natural and waste waters [4,5].

This work focuses on the complexation ability of 5,6-diphenyl-3-(2-pyridyl)-1,2,4-triazine towards Cu^{2+} . Some Cu(II) complexes of dppt have been prepared previously and studied as potential catalytically active redox agents [6].

Here we present synthesis, spectroscopic and structural data for $[\text{CuCl}_2(\text{dppt})]$ (**1**), $[\text{CuCl}_2(\text{dppt})_2] \cdot 2\text{MeOH}$ (**2**), $[\text{Cu}(\text{dppt})_2(\text{H}_2\text{O})_2](\text{NO}_3)_2$ (**3**) and $[\text{Cu}(\text{SO}_4)(\text{dppt})(\text{H}_2\text{O})]_n \cdot n\text{H}_2\text{O}$ (**4**) complexes.

The electronic structure of **1** has been calculated with the density functional theory (DFT), and TDDFT/PCM calculations have been employed to produce a hundred of doublet excited-states starting from the optimized geometry.

Currently density functional theory (DFT) is commonly used to examine the electronic structure of transition metal complexes. It meets with the requirements of being accurate, easy to use and fast enough to allow the study of relatively large molecules of transition metal complexes [7]. Recent calculations with TD-DFT method for open-shell of metal complexes (including copper complexes) have also supported the TD-DFT method to be applicable for such systems giving good assignment of experimental spectra [8,9].

2. Experimental

2.1. General procedure

All the reagents used to the synthesis were commercially available and were used without further purification.

* Corresponding author.

E-mail addresses: basia@ich.us.edu.pl (B. Machura), rafal.kruszynski@p.lodz.pl (R. Kruszynski), jmroz@wchuw.chem.uni.wroc.pl (J. Mroziński).

IR spectra were recorded on a Nicolet Magna 560 spectrophotometer in the spectral range 4000–400 cm^{-1} with the samples in the form of KBr pellets. Electronic spectra were measured on a spectrophotometer Lab Alliance UV–VIS 8500 in the range 1100–180 nm in methanol solution. Elemental analyses (C H N) were performed on a Perkin–Elmer CHN-2400 analyzer. EPR spectra were recorded at room temperature and 77 K on a Bruker ESP 300 spectrometer operating at X-band equipped with an ER 035M Bruker NMR gaussmeter and HP 5350B Hewlett–Packard microwave frequency counter.

2.2. Preparation of $[\text{CuCl}_2(\text{dppt})]$ (**1**)

A solution of dppt (0.58 mmol, 0.18 g) in methanol (15 ml) was added to 0.10 g (0.58 mmol) of $\text{CuCl}_2 \cdot 2\text{H}_2\text{O}$ in 10 ml of methanol and stirred for 2 h. The resulting solution was kept for evaporation at room temperature, and after a few days dark red crystals were obtained, filtered off and dried. Yield 75%.

Anal. Calc. for $\text{C}_{20}\text{H}_{14}\text{N}_4\text{Cl}_2\text{Cu}$: C, 54.01; H, 3.17; N, 12.60. Found: C, 54.70; H, 3.46; N, 12.35%.

IR (KBr; ν/cm^{-1}): 1603(m) and 1515(s), $\nu_{\text{C}=\text{N}}$ and $\nu_{\text{N}=\text{N}}$.

UV–Vis (MeOH; λ_{max} [nm] (ϵ ; [$\text{dm}^3 \text{mol}^{-1} \text{cm}^{-1}$])): 775.0 (100), 445.8 (50), 328.4 (36500), 302.8 (59750), 242.4 (38910) and 204.8 (90870).

2.3. Preparation of $[\text{CuCl}_2(\text{dppt})_2] \cdot 2\text{MeOH}$ (**2**)

A procedure similar to that for $[\text{CuCl}_2(\text{dppt})]$ was used with $\text{CuCl}_2 \cdot 2\text{H}_2\text{O}$ (0.10 g, 0.58 mmol) and dppt (0.36 g, 1.16 mmol). Green crystals of **2** were collected in 80% yield.

Anal. Calc. for $\text{C}_{42}\text{H}_{36}\text{N}_8\text{Cl}_2\text{O}_2\text{Cu}$: C, 61.58; H, 4.43; N, 13.68. Found: C, 60.95; H, 4.68; N, 13.20%.

IR (KBr; ν/cm^{-1}): 3361(br) $\nu_{\text{O}-\text{H}}$; 1607(m) and 1519(s) ν_{CN} and $\nu_{\text{N}=\text{N}}$.

UV–Vis (MeOH; λ_{max} [nm] (ϵ ; [$\text{dm}^3 \text{mol}^{-1} \text{cm}^{-1}$])): 769.0 (225), 507.6 (115), 339.4 (22600), 304.0 (35770) and 214.0 (68125).

2.4. Preparation of $[\text{Cu}(\text{dppt})_2(\text{H}_2\text{O})_2](\text{NO}_3)_2$ (**3**)

A solution of dppt (0.80 mmol, 0.25 g) in methanol (10 ml) was added to 0.10 g (0.40 mmol) of $\text{Cu}(\text{NO}_3)_2 \cdot 3\text{H}_2\text{O}$ in 10 ml of water and stirred for 4 h. The resulting green precipitate was filtered off and recrystallized from methanol. Crystalline precipitate of **3** was collected in 70% yield.

Anal. Calc. for $\text{C}_{40}\text{H}_{32}\text{N}_{10}\text{O}_8\text{Cu}$: C, 56.90; H, 3.82; N, 16.59. Found: C, 57.35; H, 3.98; N, 16.25%.

IR (KBr; ν/cm^{-1}): 3473(br) $\nu_{\text{O}-\text{H}}$; 1600(w), 1530(s) and 1514(m) ν_{CN} and $\nu_{\text{N}=\text{N}}$; 1384 cm^{-1} (ν_{NO_3}).

UV–Vis (MeOH; λ_{max} [nm] (ϵ ; [$\text{dm}^3 \text{mol}^{-1} \text{cm}^{-1}$])): 676.1 (180), 479.9 (155), 340.1 (26460), 300.3 (46590), 240.7 (33920) and 205.7 (85180).

2.5. Preparation of $[\text{Cu}(\text{SO}_4)(\text{dppt})(\text{H}_2\text{O})_n] \cdot n\text{H}_2\text{O}$ (**4**)

A solution of dppt (0.40 mmol, 0.12 g) in methanol (15 ml) was added to 0.10 g (0.40 mmol) of $\text{CuSO}_4 \cdot 5\text{H}_2\text{O}$ in 10 ml of water and stirred for 4 h. The resulting green precipitate was filtered off and recrystallized from methanol. Crystalline precipitate of **4** was collected in 65% yield.

Anal. Calc. for $\text{C}_{20}\text{H}_{18}\text{N}_4\text{O}_6\text{SCu}$: C, 47.48; H, 3.59; N, 11.07. Found: C, 47.77; H, 3.33; N, 11.85%.

IR (KBr; ν/cm^{-1}): 3650(m) and 3433(br) $\nu_{\text{O}-\text{H}}$; 1606(br) and 1521(s) $\nu_{\text{C}=\text{N}}$ and $\nu_{\text{N}=\text{N}}$; 1196, 1156(sh), 1129, 1021, 934 and 611 cm^{-1} (ν_{SO_4}).

UV–Vis (MeOH; λ_{max} [nm]): 682.3, 464.5, 331.2, 300.9, 240.5 and 202.8.

2.6. Crystal structures determination and refinement

The X-ray intensity data of **1**, **2**, **3** and **4** were collected on a KM-4-CCD automatic diffractometer equipped with CCD detector and graphite monochromated Mo $K\alpha$ radiation ($\lambda = 0.71073 \text{ \AA}$). Details concerning crystal data and refinement are given in Table 1. Lorentz, polarization and numerical absorption correction [10] were applied. The structures were solved by the partial structure expansion method and subsequently completed by the difference Fourier recycling. All the non-hydrogen atoms were refined anisotropically using full-matrix, least-squares technique. The hydrogen atoms were founded from the difference Fourier syntheses and were treated as, “riding” on their adjacent atoms and assigned isotropic temperature factors equal 1.2 times the value of equivalent temperature factor of the aromatic parent atoms and equal 1.5 times the value of equivalent temperature factor of the methyl parent

Table 1
Crystal data and structure refinement for **2**, **3** and **4** complexes

	2	3	4
Empirical formula	$\text{C}_{42}\text{H}_{36}\text{Cl}_2\text{N}_8\text{O}_2\text{Cu}$	$\text{C}_{40}\text{H}_{32}\text{N}_{10}\text{O}_8\text{Cu}$	$\text{C}_{20}\text{H}_{18}\text{N}_4\text{O}_6\text{SCu}$
Formula weight	819.23	844.30	505.98
Temperature (K)	291.0(3)	150(1)	291.0(3)
Wavelength (\AA)	0.71073	0.71073	0.71073
Crystal system	monoclinic	monoclinic	triclinic
Space group	$C2/c$	$P2_1/n$	$P\bar{1}$
Unit cell dimensions			
<i>a</i> (\AA)	15.285(3)	8.4621(6)	7.0084(6)
<i>b</i> (\AA)	8.286(2)	6.4346(5)	10.1467(9)
<i>c</i> (\AA)	31.414(6)	34.2110(2)	15.2168(14)
α ($^\circ$)			93.711(7)
β ($^\circ$)	93.30(3)	93.200(6)	94.531(7)
γ ($^\circ$)			104.345(7)
Volume (\AA^3)	3972.0(14)	1859.9(2)	1041.10(16)
<i>Z</i>	4	2	2
D_{calc} (Mg/m^3)	1.370	1.508	1.614
Absorption coefficient (mm^{-1})	0.731	0.658	1.196
<i>F</i> (000)	1692	870	518
Crystal size (mm)	$0.07 \times 0.14 \times 0.14$	$0.08 \times 0.08 \times 0.22$	$0.199 \times 0.027 \times 0.024$
θ Range for data collection	2.89–25.03	2.92–25.00	2.08–25.05
Index ranges	$-17 \leq h \leq 18$, $-6 \leq k \leq 9$, $-35 \leq l \leq 37$	$-10 \leq h \leq 6$, $-7 \leq k \leq 7$, $-40 \leq l \leq 39$	$-8 \leq h \leq 8$, $-12 \leq k \leq 11$, $-18 \leq l \leq 18$
Reflections collected	12346	11201	10501
Independent reflections (R_{int})	3494 (0.0638)	3254 (0.0450)	3684 (0.0243)
Completeness to $2\theta = 50^\circ$	99.3%	99.2%	99.9%
Maximum and minimum transmission	0.953 and 0.898	0.937 and 0.953	0.968 and 0.959
Data/restraints/parameters	3494/0/252	3254/0/268	3684/0/289
Goodness-of-fit on F^2	1.144	0.904	1.091
Final <i>R</i> indices [$I > 2\sigma(I)$]	$R_1 = 0.0679$	$R_1 = 0.0342$,	$R_1 = 0.0600$
<i>R</i> indices (all data)	$wR_2 = 0.1678$	$wR_2 = 0.0914$	$wR_2 = 0.1863$
	$R_1 = 0.1095$	$R_1 = 0.0595$	$R_1 = 0.0692$
Largest difference in peak and hole (e \AA^{-3})	$wR_2 = 0.1920$	$wR_2 = 0.0977$	$wR_2 = 0.1935$
	0.515 and -0.337	0.320 and -0.330	0.671 and -0.493

carbon atom or oxygen atom. All, except water molecule, hydrogen atoms positions were idealised after each cycle of refinement. The methyl and hydroxyl groups were allowed to rotate about their local three-fold axes. SHELXS97 [11], SHELXL97 [12] and SHELXTL [13] programs were used for all the calculations. Atomic scattering factors were those incorporated in the computer programs.

2.7. Magnetic measurement

The magnetization of the powdered sample was measured over the temperature range 1.8–300 K at magnetic field 0.5 Tesla, using a Quantum Design SQUID-based MPMSXL-5-type magnetometer. The superconducting magnet was generally operated at a field strength ranging from 0 to 5 Tesla.

The SQUID magnetometer was calibrated with the palladium rod sample. Corrections are based on subtracting the sample-holder signal and contribution χ_D estimated from the Pascal constants [14] and equal $-276 \times 10^{-6} \text{ cm}^3 \text{ mol}^{-1}$ for complex. The effective magnetic moment was calculated from the equation, $\mu_{\text{eff}} = 2.83(\chi_{\text{M}}T)^{1/2}$ (B.M.).

2.8. Computational details

The geometry of **1** was optimized without any symmetry restrictions in the doublet state using the hybrid B3LYP [15,16] functional of GAUSSIAN-03 [17]. The geometry was fully optimised in methanol utilising IEF-PCM formalism available in GAUSSIAN-03 [18]. The calculations were performed by using the LANL2DZ effective core potential (ECP) set of Hay and Wadt [19] for copper atom and the standard 6-31+G** basis for chloride and nitrogen, 6-31G* for carbon and 6-31G for hydrogen atoms.

Based on the optimized geometry, time-dependent density functional level (TDDFT) calculations were performed at the same B3LYP level and basis sets to calculate the electron transition energies [20].

3. Results and discussion

3.1. Preparation and infrared data

The complexes $[\text{CuCl}_2(\text{dppt})]$ (**1**), $[\text{CuCl}_2(\text{dppt})_2] \cdot 2\text{MeOH}$ (**2**), $[\text{Cu}(\text{dppt})_2(\text{H}_2\text{O})_2](\text{NO}_3)_2$ (**3**) and $[\text{Cu}(\text{SO}_4)(\text{dppt})(\text{H}_2\text{O})]_n \cdot n\text{H}_2\text{O}$ (**4**) were prepared in good yield by the reaction of 5,6-diphenyl-3-(2-pyridyl)-1,2,4-triazine (dppt) with the appropriate copper salt and molar ratio.

The selected frequencies observed in the IR spectra of $[\text{CuCl}_2(\text{dppt})]$ (**1**), $[\text{CuCl}_2(\text{dppt})_2] \cdot 2\text{MeOH}$ (**2**), $[\text{Cu}(\text{dppt})_2(\text{H}_2\text{O})_2](\text{NO}_3)_2$ (**3**) and $[\text{Cu}(\text{SO}_4)(\text{dppt})(\text{H}_2\text{O})]_n \cdot n\text{H}_2\text{O}$ (**4**) complexes are given in Section 2. For all the examined complexes the stretching vibrations of the C=N and N=N groups appear at considerable lower values with respect to the $\nu(\text{C}=\text{N})$ and $\nu(\text{N}=\text{N})$ of the free 5,6-diphenyl-3-(2-pyridyl)-1,2,4-triazine (dppt) supporting the coordination of the triazine and pyridyl rings to the metal ion [3]. The bands assignable to the bridging sulfate of **4** appear at 934, 1021, 1129, 1156 and 1196 cm^{-1} , whereas the band at 1384 cm^{-1} for **3** suggests the presence of uncoordinated nitrate ion. The broad bands in the range $3650\text{--}3100 \text{ cm}^{-1}$ in the IR spectra of **2**, **3** and **4** represent the existence of MeOH and H_2O [21].

3.2. Crystal structures

The crystallographic data of **2**, **3** and **4** complexes are summarized in Table 1. The details of hydrogen bonds are given in Table 2, and the molecular structures of **2**, **3** and **4** are presented in Figs. 1–3, respectively.

The complex **1** crystallises in the orthorhombic space group *Fdd2*. The coordination geometry about Cu(II) is a *trans* distorted square planar. The Cu ion is coordinated to pyridine and triazine rings of 5,6-diphenyl-3-(2-pyridyl)-1,2,4-triazine ligand and two chloride ions. As the X-ray structure of complex **1** has been recently reported by Eltayeb et al. [22] and quality of our structure is similar, the experimental data for **1** have not been included in the paper.

The copper atom of the compound **2** is located on the inversion centre and occupies special position *a* of the *C2/c* space group, thus the asymmetric unit consists of a half of complex molecule and one methanol molecule. By symmetry the environment of copper(II) ion in compound **2** adopts ideal tetragonal bipyramid geometry. The equatorial plane is formed by two pyridine and two triazine nitrogen atoms and the axial sites are occupied by two chloride ions at rather large distances of 2.7062(16), as a consequence of the Jahn–Teller effect. The two dppt ring systems are strictly coplanar and they are bound to central ion in *trans* configuration. Each complex molecule is connected *via* medium strength [23,24] O–H...Cl intermolecular hydrogen bonds with two solvent molecules.

The copper atom of the compound **3** is located on the inversion centre and occupies special position *b* of the *P2₁/n* space group, thus the asymmetric unit consists of a half of complex cation and one nitrate anion. The overall complex molecule conformation of compound **3** is very similar to these of compound **2**. By symmetry the environment of copper(II) ion adopts ideal tetragonal bipyramid geometry. The equatorial plane is formed by two pyridine and two triazine nitrogen atoms and the axial sites are occupied by two water molecules at rather large distances of 2.3403(19) Å, as a consequence of the Jahn–Teller effect. The two dppt ring systems are strictly coplanar and they are bound to central ion in *trans* configuration. The medium strength O–H...O intermolecular hydrogen bonds of compound **3** joins the molecules to form of hydrogen bonded chain along crystallographic *b*-axis.

All atoms of compound **4** lie in general positions, but the inversion centres located at respectively special positions *d* and *f* of the *P1* space group expand the molecule to the one dimensional, ladder type, polymer along crystallographic *a*-axis (the asymmetric unit consists of one Cu^{2+} cation one SO_4^{2-} anion one ligand, one coordinated and one uncoordinated water molecule). Each copper(II) ion is six-coordinate and their coordination geometries are best described as distorted tetragonal bipyramid with the equatorial plane defined by two nitrogen and two oxygen atoms (maximum deviation from the weighted least squares N(2), N(4), O(1), O(2) plane exists for N(4) atom and it is equal to 0.127(2) Å) with copper atom displaced 0.000(2) Å from above mentioned the weighted least squares plane. The $\text{Cu}(\text{dppt})(\text{H}_2\text{O})$ units are linked by two μ -sulfate–O,O' bridges forming planar by symmetry Cu_2O_2

Table 2
Hydrogen bonds for **2**, **3** and **4** complexes

D–H...A	H...A (Å)	D...A (Å)	D–H...A (°)	Symmetry code of A
Complex 2				
O(99)–H(99)...Cl(1)	2.42	3.165(9)	152.5	
Complex 3				
O(4)–H(4O)...O(1)	1.93	2.783(3)	151.9	<i>x, y + 1, z</i>
O(4)–H(4P)...O(3)	1.97	2.845(3)	150.7	$-x + 1, -y + 1, -z$
Complex 4				
O(1)–H(1O)...O(4)	1.82	2.760(5)	159.2	
O(1)–H(1P)...O(3)	1.63	2.600(5)	164.8	$-x + 1, -y + 2, -z + 1$
O(99)–H(99P)...O(5)	2.08	2.924(8)	179.4	

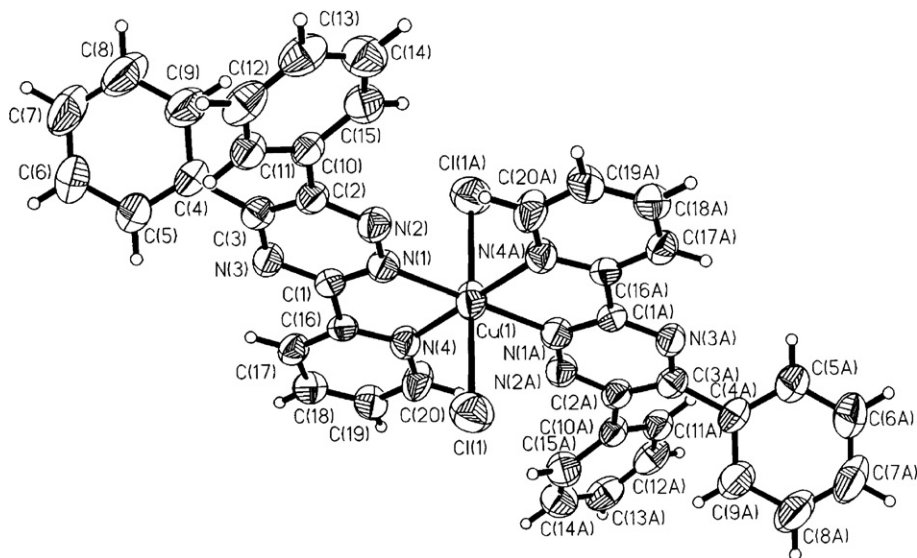


Fig. 1. The molecular structure of **2**. Displacement ellipsoids are drawn at 50% probability.

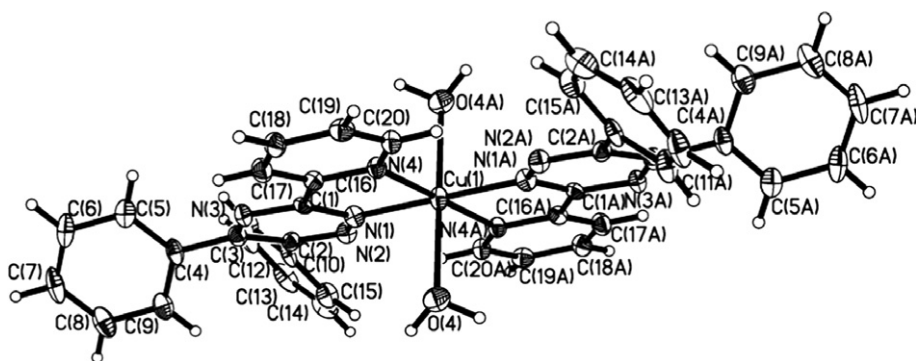


Fig. 2. The molecular structure of the cation $[\text{Cu}(\text{dppt})_2(\text{H}_2\text{O})_2]^{2+}$ in the structure **3**. Displacement ellipsoids are drawn at 50% probability.

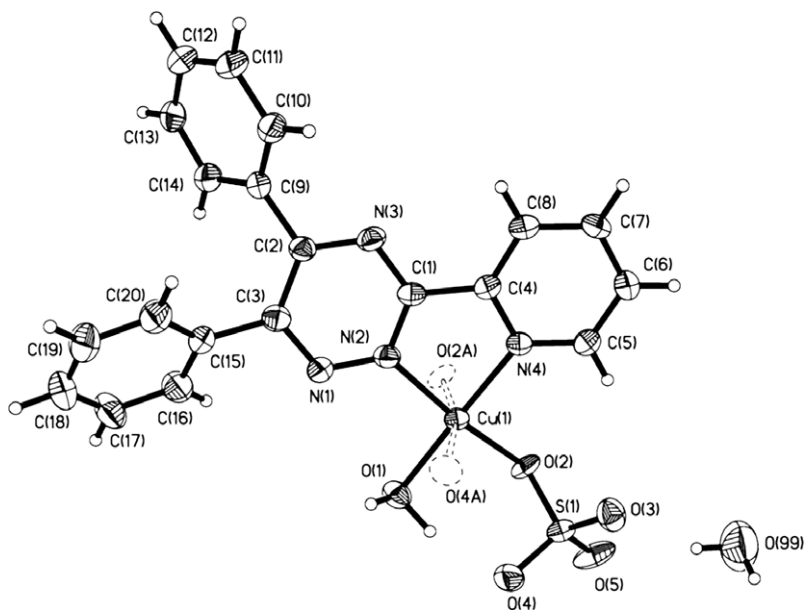


Fig. 3a. Atoms forming asymmetry unit of **4**. Displacement ellipsoids are drawn at 50% probability. The symmetry generated atoms bonded to the asymmetry unit atoms are indicated by dashed lines.

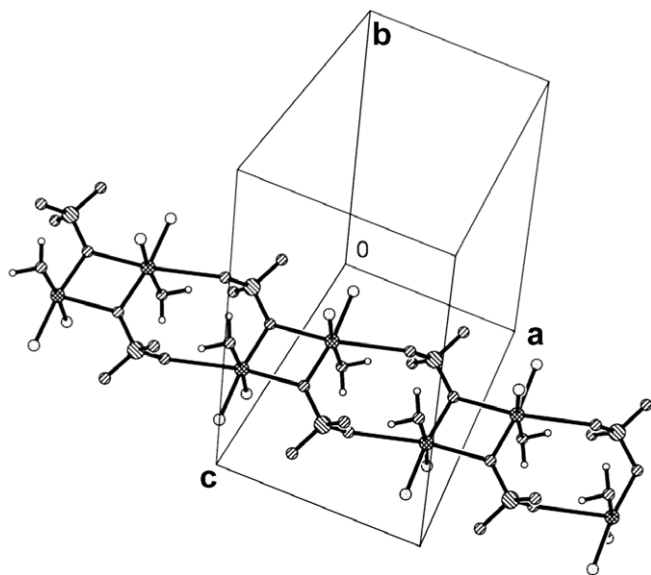


Fig. 3b. The fragment of polymer chain **4**. Atoms not involved in the chain are deleted for clarity. The copper atoms are cross-hatched, the sulphur atoms are backslashed, the oxygen atoms are slashed and nitrogen atoms are dotted.

moiety with two short [1.966(3) Å] and two longer Cu–O distances [2.367(3) Å], two bridging Cu–O–Cu angles of 100.49(12)°, leading to a Cu···Cu separation of 3.3411(11) Å. The sulfate oxygen O(4) is further coordinated to the copper atom of another binuclear unit, resulting in a polymeric structure created by the four-membered Cu₂O₂ and eight-membered Cu₂O₄S₂ rings in the spiro arrangement (in the second ring the Cu···Cu distance is 4.8865(11) Å). The structures with two bridging modes for the sulfate groups (μ -O,O' and μ -O,O), in the same complex are unique. However, a similar arrangement was observed for the [Cu₄(TPPNOL)₂(μ -SO₄)₂](ClO₄)₂ [HTPPNOL (*N,N,N*O-tris-(2-pyridylmethyl)-1,3-diaminopropan-2-ol)] complex reported by Fernandes and co-workers [25]. Different bridging modes for the sulfate groups are reflected in the different S–O bond lengths: 1.523(3) Å for S(1)–O(1) and 1.459(4) Å for S(1)–O(4). The solvent water molecule is connected to complex molecule *via* medium strength O–H···O hydrogen bond. The polymer chain is stabilised by medium strength O–H···O intramolecular hydrogen bonds.

The selected bond distances and angles of **2**, **3** and **4** are collected in Tables 3–5. The bite angle of, 6-diphenyl-3-(2-pyridyl)-1,2,4-triazine ranges from 78.99(14)° to 81.19(15)°, and is similar to that reported for the related [Cu(dppt)₂(H₂O)₂](ClO₄)₂ complex [79.7(2)°] [6].

For all three complexes, there is no significant difference between Cu–N (pyridine) and Cu–N (triazine) bond lengths, revealing that the two nitrogens are equal in donor strength. The Cu–N bond distances of mononuclear compounds are slightly longer than those in the polymer structure suggesting that the Cu–N bonds

Table 3
The experimental bond lengths (Å) and angles (°) for **2**

Bond lengths	Experimental	Bond angles	Experimental
Cu(1)–N(1)	2.023(4)	N(1)–Cu(1)–N(4)#1	101.01(14)
Cu(1)–N(4)	2.049(4)	N(1)–Cu(1)–N(4)	78.99(14)
Cu(1)–Cl(1)	2.7062(16)	N(1)–Cu(1)–Cl(1)#1	87.22(11)
		N(1)–Cu(1)–Cl(1)	92.78(11)
		N(4)–Cu(1)–Cl(1)	90.88(11)
		N(4)–Cu(1)–Cl(1)#1	89.12(11)
		N(1)#1–Cu(1)–Cl(1)	87.22(11)

#1: $-x + 1, -y, -z$.

Table 4
The experimental bond lengths (Å) and angles (°) for **3**

Bond lengths	Experimental	Bond angles	Experimental
Cu(1)–N(1)	2.028(2)	N(1)–Cu(1)–N(4)	79.84(8)
Cu(1)–N(4)	2.062(2)	N(1)#1–Cu(1)–N(4)	100.16(8)
Cu(1)–O(4)	2.3403(19)	N(1)–Cu(1)–O(4)#1	89.30(8)
		N(1)–Cu(1)–O(4)	90.70(8)
		N(4)–Cu(1)–O(4)	84.93(7)
		N(4)–Cu(1)–O(4)#1	95.07(7)

#1: $-x + 1, -y + 1, -z$.

Table 5
The experimental bond lengths (Å) and angles (°) for **4**

Bond lengths	Experimental	Bond angles	Experimental
Cu(1)–O(1)	1.951(3)	O(1)–Cu(1)–O(2)	88.50(14)
Cu(1)–O(2)	1.966(3)	O(1)–Cu(1)–N(2)	96.97(15)
Cu(1)–O(2)#1	2.367(3)	O(1)–Cu(1)–N(4)	172.52(14)
O(2)–Cu(1)#1	2.367(3)	O(2)–Cu(1)–N(4)	94.23(15)
Cu(1)–N(2)	1.996(4)	O(2)–Cu(1)–N(2)	171.29(14)
Cu(1)–N(4)	1.995(4)	N(4)–Cu(1)–N(2)	81.19(15)
S(1)–O(2)	1.523(3)	O(2)–Cu(1)–O(2)#1	79.51(13)
S(1)–O(3)	1.464(3)	O(1)–Cu(1)–O(2)#1	93.58(12)
S(1)–O(4)	1.459(4)	N(4)–Cu(1)–O(2)#1	93.76(14)
S(1)–O(5)	1.455(4)	N(2)–Cu(1)–O(2)#1	93.34(13)
		Cu(1)–O(2)–Cu(1)#1	100.49(12)

#1: $-x + 2, -y + 2, -z + 1$.

in **1**, **2** and **3** complexes are comparatively weaker. However, all the Cu–N bond lengths are consistent with those found in related systems [26].

3.3. Magnetic properties

The magnetic properties of the complex **4** were determined over the temperature range 1.8–300 K at magnetic field 0.5 Tesla. The experimental data, plotted as temperature variations of the χ_M^{-1} and $\chi_M T$, are shown in Fig. 4.

The value $\chi_M T$ at of 300 K for complex equals 0.415 cm³ mol⁻¹ K (1.82 B.M.). The value of $\chi_M T$ product increases slightly with temperature lowering and reaches 0.425 cm³ mol⁻¹ K (1.85 B.M.) value at 1.8 K.

The values of the Curie and Weiss constants determined from the relation $1/\chi_M = f(T)$ over temperature range 1.8–300 K are equal

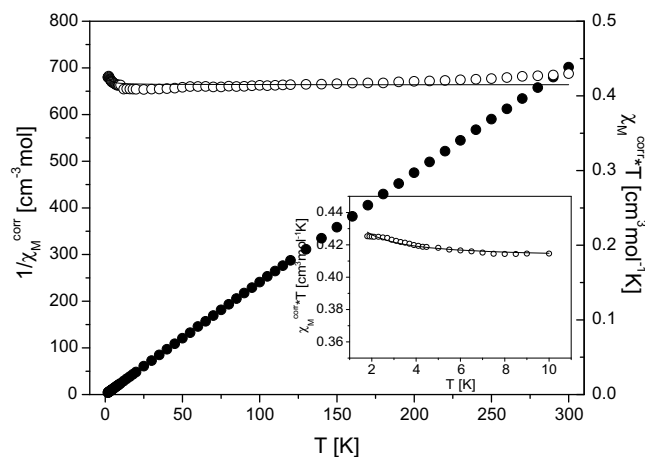
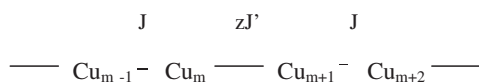


Fig. 4. Temperature dependence of experimental χ_M^{-1} (●) and $\chi_M T$ (○) for complex **4**. The inset shows dependence $\chi_M T$ vs. T (○) in the lowest temperature range. The solid line is the calculated curve for $\chi_M T$.

to $0.415 \text{ cm}^3 \text{ mol}^{-1} \text{ K}$ and 0.04 K , respectively. A very small, positive value of Weiss constant confirms the occurrence of very weak ferromagnetic interactions between the copper centers in the dimer.

The molecular structure of $[\text{Cu}(\text{SO}_4)(\text{dppt})(\text{H}_2\text{O})]_n \cdot n\text{H}_2\text{O}$ (**4**) (Fig. 4b) suggests the magnetic exchange interactions in alternating chain:



where J and zJ' are the exchange parameters via (–O–) and (–O–S–O–) bridges, respectively.

The path of the magnetic interaction between Cu^{II} centers inside eight-membered ($\text{Cu}_2\text{O}_4\text{S}_2$) ring is considerably longer than inside four-membered (Cu_2O_2) ring. For that reason the dimer model with pairwise interactions may be used as a good approximation [27]. Hamiltonian $H = -2J\vec{S}_1 \cdot \vec{S}_2$ for $S_1 = S_2 = 1/2$ leads to the Bleaney–Bowers expression (1) [28]. To elucidate the significance of exchange between dimeric subunits in the chain, a molecular field correction term was also included (Eq. (2)) [29]

$$\chi_M = \frac{2N\beta^2 g^2}{3kT} \left[1 + \frac{1}{3} \exp(-2J/kT) \right] \quad (1)$$

$$\chi_M^{\text{corr}} = \frac{\chi_M}{1 - \frac{2zJ'}{N\beta^2 g^2} \cdot \chi_M} \quad (2)$$

where N is the Avogadro's number, g – the spectroscopic splitting factor, β – the Bohr magneton, k – the Boltzmann constant, J – exchange parameter and zJ' – molecular field correction (interdimer interaction). The least-squares fit of the experimental data using these equations was limited to the temperature range from 1.8 K up to 300 K and leads to singlet–triplet ($2J$) separation value equals 0.20 cm^{-1} , $g = 2.10$ and $zJ' = 0$, as indicated by the solid curve in Fig. 5. The agreement factor R is equal 4.02×10^{-5} . The criterion used in determination of the best fit was based on minimization of the sum of squares of the deviation:

$$R = \sqrt{\sum_{i=1}^n \frac{1}{(\chi_i^{\text{exp}})^2} (\chi_i^{\text{exp}} - \chi_i^{\text{calc}})^2} / \sqrt{\sum_{i=1}^n \frac{1}{(\chi_i^{\text{exp}})^2}}$$

Magnetic interaction in the dimeric copper compound strongly depends on Cu–O–Cu angle. For angles close to 97° it is possible to found accidental orthogonality and consequently, J values ~ 0 or positive [30,31]. The weak ferromagnetic interactions between the copper centers in the dimeric

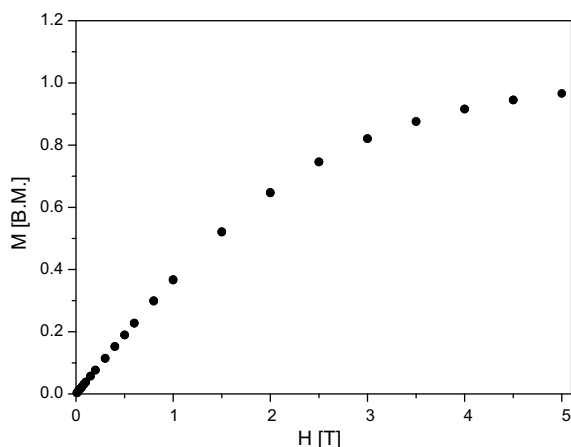


Fig. 5. Field dependence of the magnetization for complex **4**.

subunits (Cu_2O_2) arise from the value of bridging angle $\text{Cu}(1)\text{--O}(2)\text{--Cu}(1)\#1$ ($100.49(12)^\circ$) [31].

Results of the calculations on the magnetic data indicated only very weak ferromagnetic interaction between copper centers inside four-membered (Cu_2O_2) rings with value of the singlet–triplet separation $2J = +0.2 \text{ cm}^{-1}$. The value of molecular field corrections ($zJ' = 0$) indicated total magnetic isolation of the four-membered rings in the crystal lattice.

The variation of the magnetization M versus the magnetic field H for complex **4** at 2 K was shown in Fig. 5. As the magnetic field increases, the M versus H curve indicates linear relation up to $\sim 1 \text{ T}$ and then shows a sinusoidal variation up to 5 T near saturation value at $M = 0.97 \text{ B.M.}$

3.4. EPR spectra

The EPR powder spectra of the complex **4** (Fig. 6) recorded in the X-band at room temperature, 77 K and 4.2 K indicate two poorly resolved lines related to $g_{\perp} = 2.08$ and $g_{\perp} = 2.21$ parameters. The observed EPR spectrum is the average spectrum of two copper centers in the ligand field of the distorted tetragonal–bipyramidal symmetry $\text{Cu}(1)\text{N}_2\text{O}_4$ and $\text{Cu}(2)\text{N}_2\text{O}_4$, respectively.

3.5. Geometry optimisation

The geometry of **1** was optimised in a doublet state by the DFT method with the B3LYP functional. The optimized geometric parameters of **1** are gathered in Table 6. In general, the predicted bond lengths and angles are in agreement with the values based upon the X-ray crystal structure data, and the general trends observed in the experimental data are well reproduced in the calculations.

3.6. Electronic spectra

The experimental electronic spectra of **1**, **2**, **3** and **4** are presented in Fig. 7. The positions of absorption bands and values of molar absorption coefficients for the complexes are given in the Experimental Part. As can be seen from Fig. 7 the UV/Vis spectra are rather indistinctive for molecular structure determination. For all the complexes the visible region exhibit broad poorly resolved absorption bands with maxima at 775.0 and 445.8 nm for **1**, 769.0 and 507.6 nm for **2**, 676.1 and 479.9 nm for **3** and 682.3 and 464.3 nm for **4**. The UV spectra of the **1**, **2**, **3** and **4** are also very similar in terms of the position, intensity and shape of the bands.

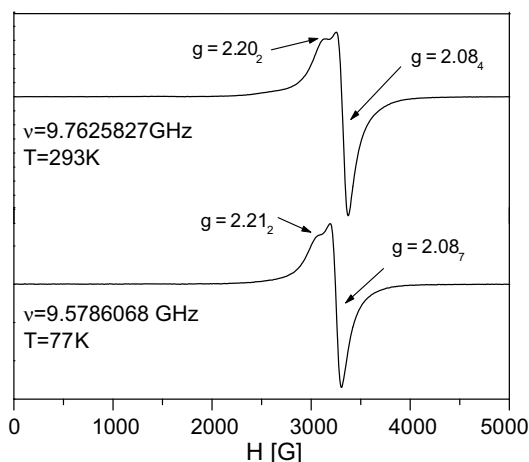
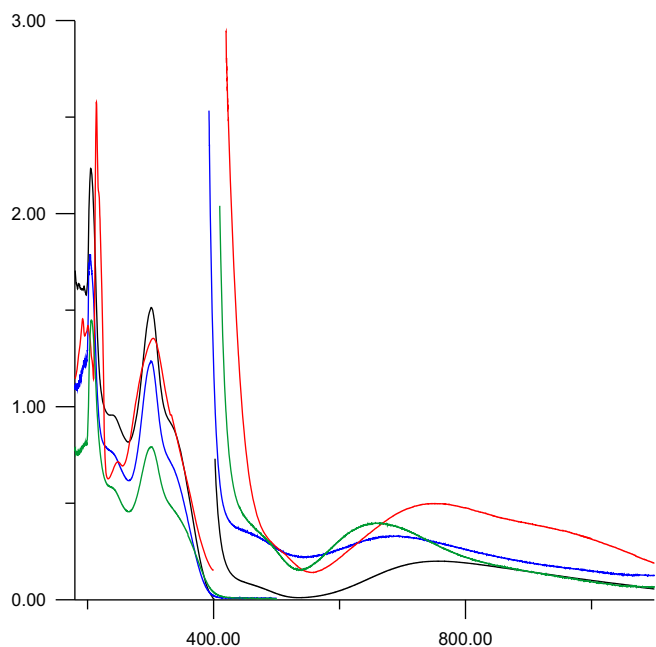


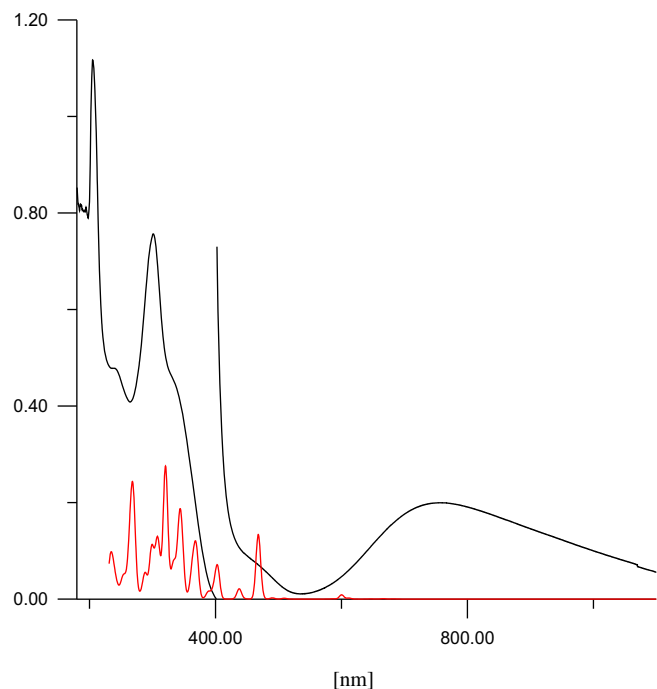
Fig. 6. EPR (X-band) spectrum of powdered **4** at room temperature and 77 K .

Table 6
The optimized bond lengths (Å) and angles (°) for **1**

Bond lengths	Optimized	Bond angles	Optimized
Cu(1)–N(2)	2.067	N(4)–Cu(1)–N(2)	79.47
Cu(1)–N(4)	2.073	N(2)–Cu(1)–Cl(1)	173.71
Cu(1)–Cl(1)	2.344	N(4)–Cu(1)–Cl(1)	94.51
Cu(1)–Cl(2)	2.325	N(2)–Cu(1)–Cl(2)	94.14
		N(4)–Cu(1)–Cl(2)	173.65
		Cl(2)–Cu(1)–Cl(1)	91.82

**Fig. 7.** The experimental electronic absorption spectra of **1** (black), **2** (red), **3** (green) and **4** (blue). (For interpretation of the references to colour in this figure legend, the reader is referred to the web version of this article.)**Table 7**
The calculated electronic transitions and their assignments to the experimental absorption bands of **1**

The most important orbital excitations	Character	λ (nm)	E (eV)	f	Experimental λ (nm)	
H-5(β) \rightarrow L(β)	$\pi(\text{Cl})/\pi(\text{dppt})/d \rightarrow d$	682.2	1.82	0.0004	775.0	
H-8(β) \rightarrow L(β)	$\pi(\text{Cl})/d \rightarrow d$	666.5	1.86	0.0008		
H(β) \rightarrow L(β)	$\pi(\text{dppt}) \rightarrow d$	646.6	1.92	0.0003		
H-14(β) \rightarrow L(β)	$d/\pi(\text{dppt}) \rightarrow d$	611.8	2.03	0.0021		
H-3(β) \rightarrow L(β)	$\pi(\text{Cl}) \rightarrow d$	600.3	2.07	0.0088		
H(β) \rightarrow L(β)	$\pi(\text{dppt}) \rightarrow d$	586.6	2.11	0.0005		
H-2(β) \rightarrow L(β)	$\pi(\text{dppt}) \rightarrow d$	471.1	2.63	0.0144		445.8
H-4(β) \rightarrow L(β)	$\pi(\text{dppt})/\pi(\text{Cl}) \rightarrow d$	467.6	2.65	0.1251		
H-6(β) \rightarrow L(β)	$\pi(\text{Cl})/\pi(\text{dppt})/d \rightarrow d$	437.2	2.84	0.0138		
H-8(β) \rightarrow L(β)	$\pi(\text{Cl})/\pi(\text{dppt})/d \rightarrow d$	403.0	3.08	0.0659		
H(α) \rightarrow L + 1(α) H(β) \rightarrow L + 2(β)	$\pi(\text{dppt}) \rightarrow \pi^*(\text{dppt})$	369.6	3.35	0.0920	328.4	
H(β) \rightarrow L + 2(β)	$\pi(\text{dppt}) \rightarrow \pi^*(\text{dppt})$	364.7	3.40	0.0500		
H-1(α) \rightarrow L(α)	$\pi(\text{dppt}) \rightarrow \pi^*(\text{dppt})$	361.9	3.42	0.0212		
H-3(α) \rightarrow L(α)	$\pi(\text{dppt}) \rightarrow \pi^*(\text{dppt})$	347.3	3.57	0.0515	302.8	
H-2(β) \rightarrow L + 1(β)	$\pi(\text{dppt}) \rightarrow \pi^*(\text{dppt})$	345.5	3.59	0.0501		
H-11(β) \rightarrow L(β)	$\sigma(\text{Cl}) \rightarrow d$	342.3	3.62	0.1187		
H-1(β) \rightarrow L + 2(β)	$\pi(\text{dppt}) \rightarrow \pi^*(\text{dppt})$	333.1	3.72	0.0489		
H-2(β) \rightarrow L + 2(β)	$\pi(\text{dppt}) \rightarrow \pi^*(\text{dppt})$	320.8	3.86	0.1641		
H-2(β) \rightarrow L + 2(β)	$\pi(\text{dppt}) \rightarrow \pi^*(\text{dppt})$	319.4	3.88	0.0789		
H-12(β) \rightarrow L(β)	$\sigma(\text{Cl}) \rightarrow d$	308.7	4.02	0.0697		
H-5(α) \rightarrow L + 2(α)	$\pi(\text{Cl})/\pi(\text{dppt}) \rightarrow \pi^*(\text{dppt})$	298.4	4.16	0.0990		
H-7(β) \rightarrow L + 2(β)	$\pi(\text{Cl})/\pi(\text{dppt})/d \rightarrow \pi^*(\text{dppt})$	269.6	4.60	0.1032		242.4
H-16(β) \rightarrow L(β)	$n(\text{dppt})/\sigma(\text{Cl})/d \rightarrow d$	269.4	4.60	0.0626		
H-8(β) \rightarrow L + 2(β)	$\pi(\text{Cl})/d \rightarrow \pi^*(\text{dppt})$	265.9	4.66	0.0481	204.8	
H-8(β) \rightarrow L + 2(β)	$\pi(\text{Cl})/d \rightarrow \pi^*(\text{dppt})$	264.8	4.68	0.0647		

 f – oscillator strength; H – highest occupied molecular orbital; L – lowest unoccupied molecular orbital.**Fig. 8.** The experimental (black) and calculated (red) electronic absorption spectra of **1**. (For interpretation of the references to colour in this figure legend, the reader is referred to the web version of this article.)

For complex **1** the nature of the transitions observed in the UV–Vis spectra has been studied by the time-dependent density functional (TDDFT) method. The calculated electronic spectrum of **1** in comparison with the experimental one is presented in Fig. 8. Each calculated transition is represented by a gaussian function $y = ce^{-bx^2}$ with the height (c) equal to the oscillator strength and b equal to 0.04 nm^{-2} .

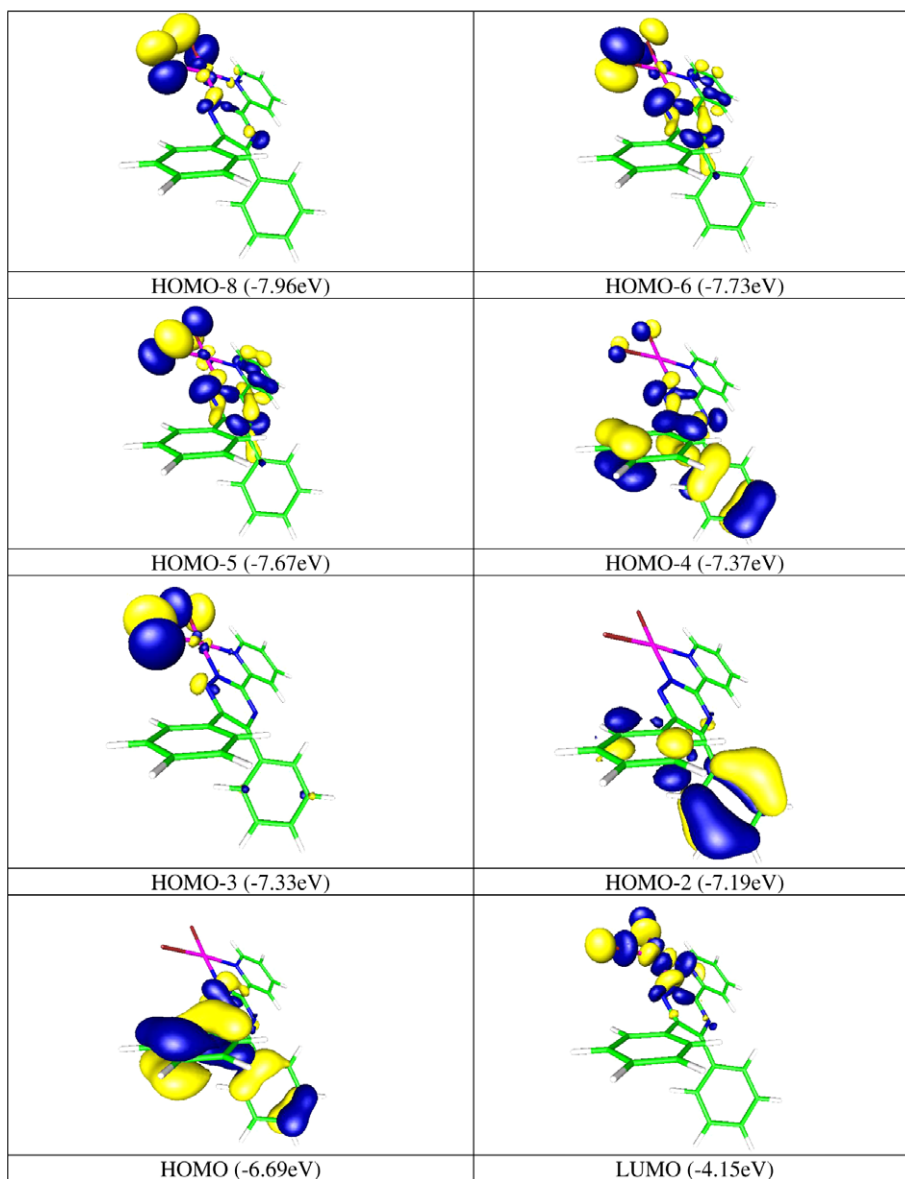


Fig. 9. Contour plots and energy of the selected β -spin HOMO and β -spin LUMO orbitals active in the electronic transitions for complex **1**. The orbitals were plotted with contour values -0.04 (yellow) and 0.04 au (blue). (For interpretation of the references to colour in this figure legend, the reader is referred to the web version of this article.)

Table 7 presents the calculated spin allowed electronic transitions of **1** and their assignments to the experimental bands. For the high energy part of the spectrum, only transitions with oscillator strengths larger than 0.500 are listed in Table 7. The assignment of the calculated orbital excitations to the experimental bands was based on an overview of the contour plots and relative energy to the orbitals HOMO and LUMO involved in the electronic transitions. The several contours of occupied and unoccupied MOs (active in the electronic transitions) of **1** are presented in Fig. 9.

The TDDFT/PCM calculations show that the two longest wavelength experimental bands of **1** at 775.0 and 445.8 nm originate in the transitions between some lowest β -spin HOMO orbitals and β -spin LUMO orbital. As can be seen from the Fig. 9, the LUMO orbital with β -spin is mainly Cu $d_{x^2-y^2}$ orbital in character, the β -spin HOMO and HOMO–1 orbitals are composed of the π -bonding orbitals of 5,6-diphenyl-3-(2-pyridyl)-1,2,4-triazine, and the HOMO–14, HOMO–8, HOMO–5 and HOMO–3 are ligand (Cl or dppt) π -bonding orbitals with some contribution of d_{Cu} orbitals. Accordingly, the transitions assigned to the two longest wavelength experimental bands can be seen as mixed Cl/dppt \rightarrow Cu

(LMCT) and $d \rightarrow d$ (LF). Thus, no ‘clear’ $d-d$ transition bands occur in the low-lying energy region for **1**. The reason for this is probably due to the fact that the dppt ligand provides high-lying occupied π -bonding orbitals, and as a result the high-lying occupied orbitals are composed of the π -bonding orbitals of 5,6-diphenyl-3-(2-pyridyl)-1,2,4-triazine.

The experimental bands at 328.4, 302.8, 242.4 and 204.8 nm are attributed to the intraligand (IL) ($\pi(\text{dppt}) \rightarrow \pi^*(\text{dppt})$) and ligand–ligand charge transfer ($\pi(\text{Cl}) \rightarrow \pi^*(\text{dppt})$) transitions.

4 Supplementary data

CCDC 684890, 684891, 684892 and 684893 contain the supplementary crystallographic data for $\text{C}_{20}\text{H}_{14}\text{N}_4\text{Cl}_2\text{Cu}$, $\text{C}_{42}\text{H}_{36}\text{Cl}_2\text{N}_8\text{O}_2\text{Cu}$, $\text{C}_{40}\text{H}_{32}\text{N}_{10}\text{O}_8\text{Cu}$ and $\text{C}_{20}\text{H}_{18}\text{N}_4\text{O}_6\text{SCu}$. These data can be obtained free of charge via <http://www.ccdc.cam.ac.uk/conts/retrieving.html>, or from the Cambridge Crystallographic Data Centre, 12 Union Road, Cambridge CB2 1EZ, UK; fax: (+44) 1223-336-033; or e-mail: deposit@ccdc.cam.ac.uk.

Acknowledgements

The GAUSSIAN03 calculations were carried out in the Wrocław Centre for Networking and Supercomputing, WCSS, Wrocław, Poland.

References

- [1] G. Garcia, I. Solano, G. Sanchez, G. Lopez, *Polyhedron* 14 (1995) 1855.
- [2] V. Béreau, J. Rey, E. Deydier, J. Marrot, *Inorg. Chim. Acta* 351 (2003) 389.
- [3] V. Béreau, J. Marrot, *CR Chim.* 8 (2005) 1087.
- [4] P.L. Croot, K.A. Hunter, *Anal. Chim. Acta* 406 (2000) 289.
- [5] J. Almog, A. Hirshfeld, B. Glattstein, J. Sterling, Z. Goren, *Anal. Chim. Acta* 322 (1996) 203.
- [6] R. Uma, M. Palaniandavar, R.J. Butcher, *J. Chem. Soc., Dalton Trans.* (1996) 2061.
- [7] H. Chermette, *Coord. Chem. Rev.* 178–180 (1998) 699.
- [8] T.K. Prasad, M.V. Rajasekharan, *Polyhedron* 26 (2007) 1364.
- [9] Y.P. Tong, S.L. Zheng, *J. Mol. Struct.* 841 (2007) 34.
- [10] STOE & Cie, X-RED, Version 1.18. STOE & Cie GmbH, Darmstadt, Germany, 1999.
- [11] G.M. Sheldrick, *Acta Crystallogr., Sect. A* 46 (1990) 467.
- [12] G.M. Sheldrick, *SHELXL97*, Program for the Refinement of Crystal Structures, University of Göttingen, Germany, 1997.
- [13] G.M. Sheldrick, *SHELXTL*: Release 4.1 for Siemens Crystallographic Research Systems, 1990.
- [14] E. König, *Magnetic Properties of Coordination and Organometallic Transition Metal Compounds*, Springer-Verlag, Berlin, 1966.
- [15] A.D. Becke, *J. Chem. Phys.* 98 (1993) 5648.
- [16] C. Lee, W. Yang, R.G. Parr, *Phys. Rev. B* 37 (1988) 785.
- [17] M.J. Frisch, G.W. Trucks, H.B. Schlegel, G.E. Scuseria, M.A. Robb, J.R. Cheeseman, J.A. Montgomery Jr., T. Vreven, K.N. Kudin, J.C. Burant, J.M. Millam, S.S. Iyengar, J. Tomasi, V. Barone, B. Mennucci, M. Cossi, G. Scalmani, N. Rega, G.A. Petersson, H. Nakatsuji, M. Hada, M. Ehara, K. Toyota, R. Fukuda, J. Hasegawa, M. Ishida, T. Nakajima, Y. Honda, O. Kitao, H. Nakai, M. Klene, X. Li, J.E. Knox, H.P. Hratchian, J.B. Cross, C. Adamo, J. Jaramillo, R. Gomperts, R.E. Stratmann, O. Yazyev, A.J. Austin, R. Cammi, C. Pomelli, J.W. Ochterski, P.Y. Ayala, K. Morokuma, G.A. Voth, P. Salvador, J.J. Dannenberg, V.G. Zakrzewski, S. Dapprich, A.D. Daniels, M.C. Strain, O. Farkas, D.K. Malick, A.D. Rabuck, K. Raghavachari, J.B. Foresman, J.V. Ortiz, Q. Cui, A.G. Baboul, S. Clifford, J. Cioslowski, B.B. Stefanov, G. Liu, A. Liashenko, P. Piskorz, I. Komaromi, R.L. Martin, D.J. Fox, T. Keith, M.A. Al-Laham, C.Y. Peng, A. Nanayakkara, M. Challacombe, P.M.W. Gill, B. Johnson, W. Chen, M.W. Wong, C. Gonzalez, J.A. Pople, *GAUSSIAN 03*, Revision B.03, Gaussian, Inc., Pittsburgh, PA, 2003.
- [18] M. Cossi, V. Barone, B. Mennucci, J. Tomasi, *Chem. Phys. Lett.* 286 (1998) 253.
- [19] P.J. Hay, W.R. Wadt, *J. Chem. Phys.* 82 (1985) 299.
- [20] M.E. Casida, *Recent Developments and Applications in Modern Density Functional Theory*, in: J.M. Seminario (Ed.), *Theoretical and Computational Chemistry*, vol. 4, Elsevier, Amsterdam, 1996.
- [21] K. Nakamoto, *Infrared and Raman Spectra of Inorganic and Coordination Compounds*, 4th ed., Wiley-Interscience, New York, 1986.
- [22] N.E. Eltayeb, S.G. Teoh, H.-K. Fun, K. Ibrahim, M.M. Rosli, *Acta Crystallogr., Sect. E* 63 (2007) m1182.
- [23] G.R. Desiraju, T. Steiner, *The Weak Hydrogen Bond in Structural Chemistry and Biology*, Oxford University Press, 1999.
- [24] G.A. Jeffrey, W. Saenger, *Hydrogen Bonding in Biological Structures*, Springer-Verlag, 1994.
- [25] Ch. Fernandes, A.J. Bortoluzzi, B. Szpoganicz, E. Schwingel, A. Neves, *Inorg. Chim. Acta* 358 (2005) 997.
- [26] F.H. Allen, *Acta Crystallogr., Sect. B* 58 (2002) 380.
- [27] A. Cornia, A.C. Fabretti, F. Ferraro, D. Gatteschi, A. Giusti, *Chem. Soc., Dalton Trans.* 3363 (1993).
- [28] B. Bleaney, K.D. Bowers, *Proc. R. Soc. London, Ser. A* 214 (1952) 451.
- [29] J. Samuel Smart, *Effective Field Theories of Magnetism*, W.B. Saunders Comp., Philadelphia and London, 1966.
- [30] O. Kahn, *Molecular Magnetism*, VCH Publishers, New York, 2003.
- [31] W.H. Crawford, H.W. Richardson, J.R. Wasson, D.J. Hadgson, W.E. Hatfield, *Inorg. Chem.* 15 (1976) 2107.